AGU PUBLICATIONS

Geophysical Research Letters

RESEARCH LETTER
10.1002/2017GL072648

Key Points:
- Propagation of a large rift in Larsen C ice shelf is governed by ice shelf heterogeneity
- Plausible calving scenarios will perturb ice shelf velocity all the way to the grounding line
- Higher fracture toughness of suture zones is key to stability of ice shelves

Supporting Information:
- Supporting Information S1
- Table S1
- Table S2
- Movie S1

Correspondence to:
C. Borstad,
chris.borstad@unis.no

Citation:
Borstad, C., D. McGrath, and A. Pope (2017), Fracture propagation and stability of ice shelves governed by ice shelf heterogeneity, *Geophys. Res. Lett.*, *44*, 4186–4194, doi:10.1002/2017GL072648.

Received 14 JAN 2017
Accepted 13 APR 2017
Accepted article online 18 APR 2017
Published online 8 MAY 2017

Fracture propagation and stability of ice shelves governed by ice shelf heterogeneity

Chris Borstad[1], Daniel McGrath[2,3], and Allen Pope[4,5]

[1]Department of Arctic Geophysics, The University Centre in Svalbard, Longyearbyen, Norway, [2]Department of Geosciences, Colorado State University, Fort Collins, Colorado, USA, [3]U.S. Geological Survey Alaska Science Center, Anchorage, Alaska, USA, [4]National Snow and Ice Data Center, Cooperative Institute for Research in Environmental Sciences, University of Colorado Boulder, Boulder, Colorado, USA, [5]Polar Science Center, Applied Physics Laboratory, University of Washington, Seattle, Washington, USA

Abstract Tabular iceberg calving and ice shelf retreat occurs after full-thickness fractures, known as rifts, propagate across an ice shelf. A quickly evolving rift signals a threat to the stability of Larsen C, the Antarctic Peninsula's largest ice shelf. Here we reveal the influence of ice shelf heterogeneity on the growth of this rift, with implications that challenge existing notions of ice shelf stability. Most of the rift extension has occurred in bursts after overcoming the resistance of suture zones that bind together neighboring glacier inflows. We model the stresses in the ice shelf to determine potential rift trajectories. Calving perturbations to ice flow will likely reach the grounding line. The stability of Larsen C may hinge on a single suture zone that stabilizes numerous upstream rifts. Elevated fracture toughness of suture zones may be the most important property that allows ice shelves to modulate Antarctica's contribution to sea level rise.

Plain Language Summary The Larsen C Ice Shelf is the largest floating mass of glacier ice attached to the Antarctic Peninsula. A giant crack began growing across the ice shelf in 2014. By the end of 2016, the crack has grown in length by over 70 km. Sometime in the near future, it will release an iceberg the size of Delaware. Some scientists believe that this will be just the first in a series of cracks that may soon cause the ice shelf to shatter, just like its neighbor Larsen B in 2002. We studied this crack using satellite data from the years 2005 through 2016. We found that the crack grows in bursts, and it slows down when it reaches patches of stronger ice. We use a computer model to predict what direction the crack will grow. After the crack releases a giant iceberg, most of the remaining ice will speed up. Whether the ice shelf survives or soon shatters depends on a single, narrow stripe of strong ice that is currently preventing many additional cracks from growing across the ice shelf. If this stripe of strong ice is growing weaker, Larsen C may soon be history.

1. Introduction

The collapse of ice shelves has a significant and long-lasting impact on discharge from the Antarctic Ice Sheet, as demonstrated by the sustained glacier thinning and acceleration following the loss of ice shelves on the Antarctic Peninsula [*Rignot et al.*, 2004; *Scambos et al.*, 2004; *Berthier et al.*, 2012; *Scambos et al.*, 2014; *Wuite et al.*, 2015]. The ability to predict ice shelf collapse will be crucial for improving projections of Antarctica's contribution to future sea level rise. Climate warming has been implicated in the loss of some ice shelves, leading to the suggestion that a metric of mean annual temperature might define a geographic limit of ice shelf viability [*Mercer*, 1978; *Doake and Vaughan*, 1991]. Indeed, surface melting and hydrofracturing has been implicated [*Glasser and Scambos*, 2008; *Banwell et al.*, 2013] as the ultimate cause of the collapse of the Larsen B ice shelf in 2002, although the shelf was likely preconditioned for collapse by many years of firn densification, thinning, fracture-induced weakening, and ice front retreat [*Vieli et al.*, 2007; *Borstad et al.*, 2012].

Prevailing hypotheses of ice shelf stability involve the determination of a critical ice front position within which an ice shelf is likely to be unstable. A "compressive arch," defined along a contour where the maximum compressive strain rate decreases to zero, has been hypothesized as a limit for ice shelf viability [*Doake et al.*, 1998]. Others have hypothesized that the orientation of the maximum tensile stress with respect to the flow direction (the "stress-flow" angle) could be used to define a critical ice front position [*Kulessa et al.*, 2014;

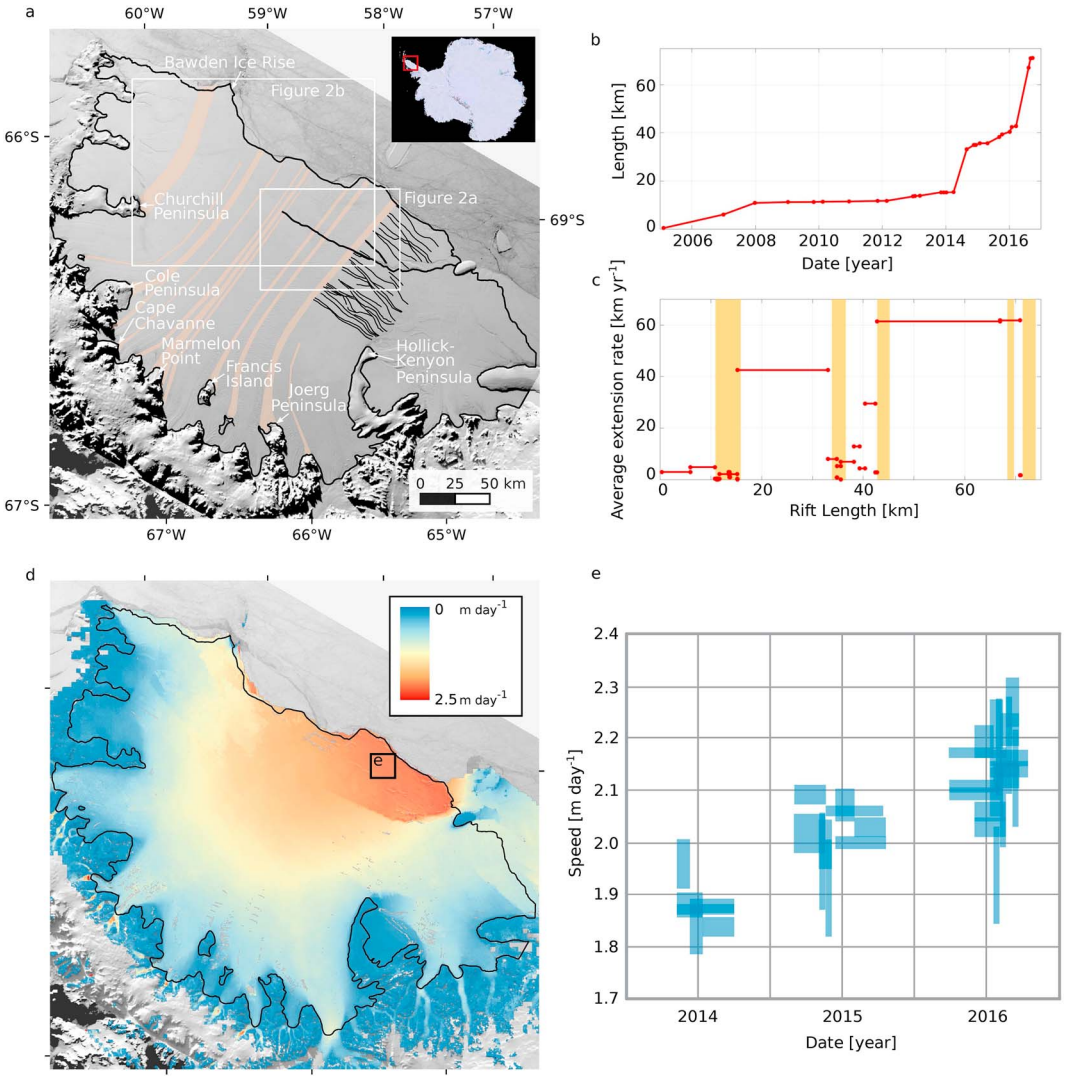

Figure 1. Observations of rift propagation and flow speed of Larsen C Ice Shelf, Antarctica. (a) Longitudinal suture zones [*Holland et al.*, 2009] overlaid on a Moderate Resolution Imaging Spectroradiometer image from 23 August 2016. Rift location on 29 September 2016 (thick line) and existing fractures (thin lines) terminating in Joerg Peninsula suture zone. (b) Rift length through time. (c) Average rift extension rate (red lines) as a function of rift length, with suture zones indicated by vertical orange bars. (d) The 2013–2016 ice flow speed from Landsat 8 image pairs. (e) Speed through time for area defined in Figure 1d. Width of boxes indicates duration of image pair; height indicates cross-correlation uncertainty.

Jansen et al., 2015]. Both notions of stability can be used to assess the potential impact of ice shelf retreat following rift propagation, since rifts define a postcalving ice front. However, neither criterion relates to factors that govern fracture propagation in the first place.

Limited observations indicate that the first-order control on rift propagation is the longitudinal glaciological stress in the ice [*Joughin and MacAyeal*, 2005]. Episodic variability in rift propagation rates [*Fricker et al.*, 2005; *Bassis et al.*, 2008; *Walker et al.*, 2015] is likely due to the presence of material heterogeneities in an ice shelf [*Hulbe et al.*, 2010; *Luckman et al.*, 2012; *McGrath et al.*, 2012a; *Jansen et al.*, 2013; *McGrath et al.*, 2014]. Key sources of ice shelf heterogeneity are longitudinal flowbands, known as suture zones, that form downstream of peninsulas and bind together neighboring meteoric inflows from tributary glaciers.

The recent growth of a large rift in the Larsen C Ice Shelf (Figure 1a) has raised concerns about possible destabilization of the shelf [*Jansen et al.*, 2015]. Although the rift may remove predominantly "passive" ice that provides limited buttressing [*Fürst et al.*, 2016], it may result in an ice front position that is conducive to further

retreat [*Jansen et al.*, 2015]. If it removes ice in contact with the Bawden Ice Rise, a critical pinning point in the northern portion of the shelf, Larsen C may rapidly destabilize [*Kulessa et al.*, 2014; *Fürst et al.*, 2016; *Borstad et al.*, 2013; *Holland et al.*, 2015]. However, predictions of the fate of the ice shelf to date have not related to the factors that destabilized the rift, nor on whether this represents an isolated or more widespread weakening of the shelf.

Here we describe the growth of this rift between early 2005 and late 2016, detail how the material heterogeneity of the shelf controls the rift propagation rate, and quantify ice shelf velocity perturbations to potential future calving events. We conclude with a discussion of the implications for the near-term stability of the shelf in the context of existing notions of ice shelf stability.

2. Methods

2.1. Rift Tip Location

We tracked the rift tip using Landsat 7 Enhanced Thematic Mapper Plus (ETM+) and 8 panchromatic imagery (15 m/pixel; see Table S3 in the supporting information for image IDs) from day of year (DOY) 42 in 2005 to DOY 273 in 2016. We purposefully avoided using other satellite platforms due to possible intersensor biases. Given widely varying illumination conditions, we applied a consistent stretch relative to observed ice shelf radiance to each image before manually picking the rift tip, identified by a shadowed surface depression (rather than open fracture). Rift length is determined by measuring the straight-line distance between the rift tip and where the rift crosses an along-flow line that marks where the rift initiated in 2005. We estimate the uncertainty in rift tip location to be 200 m based on repeated measurements by different individuals. We calculate average extension rate of the rift as the change in rift length divided by the time between subsequent satellite images. The actual instantaneous propagation rate during episodic bursts of propagation is expected to be much higher, but with sporadic cloud-free satellite coverage we are limited to determining average rates of rift extension over longer time periods.

2.2. Time-Varying Velocity Fields

We used Landsat 8 image pairs (310; Tables S1 and S2) and the feature tracking algorithm PyCorr [*Fahnestock et al.*, 2016] to produce time-varying velocity fields (gridded at 300 m) for Larsen C from late 2013 to late 2016 (Figure 1d). Using the cross-correlation algorithm's output, we filtered raw ice velocities based on the relative strength of the strongest correlation to the second strongest correlation (retaining delcorr > 0.15). In addition, we used the full stack of image pairs to filter data both spatially and temporally. We used 9 km^2 squares across all time steps to calculate the mean and standard deviation of ice velocity and subsequently removed outlier observations ($> \pm 3$ standard deviations from the mean) over three iterations. We calculated resulting mosaics by weighting image pairs based on their duration [*Fahnestock et al.*, 2016].

2.3. Numerical Modeling

Velocity observations are used to determine the state of stress of the ice shelf. We apply an inverse method [*Larour et al.*, 2005] implemented in the Ice Sheet System Model [*Larour et al.*, 2012] to calculate the spatial distribution of the flow viscosity parameter ("*B*") that minimizes the difference between modeled and observed velocities. A steady state estimate of the depth-integrated ice temperature is calculated [*Borstad et al.*, 2013] to provide an initial estimate for the viscosity parameter *B* [*Cuffey and Paterson*, 2010]. Some data gaps are present in the time-varying velocity fields, and these are filled using a nearest neighbors algorithm.

The ice shelf surface elevation and thickness are taken from a recent analysis of CryoSat-2 data from 2011 to 2014 [*Chuter and Bamber*, 2015]. Missing surface and thickness data are filled, where available, using Bedmap2 [*Fretwell et al.*, 2013], with any residual holes filled using a nearest neighbors algorithm. The firn air content, inferred from the actual ice thickness and freeboard of the ice shelf, is subtracted in order to model an equivalent solid ice thickness with density 917 kg m^{-3}. The ice shelf surface and base elevation are then adjusted to satisfy local hydrostatic equilibrium. A recent grounding line mask is adopted [*Depoorter et al.*, 2013], and local areas of grounding are defined according to a recent ice rises inventory [*Matsuoka et al.*, 2015]. In the inverse algorithm, the observed velocity is imposed in all areas where the ice is grounded.

The ice shelf is modeled at a nominal resolution of 1 km, corresponding to the resolution of the ice thickness data. An *L* curve analysis [*Morlighem et al.*, 2013] is used to determine an appropriate level of regularization for the inverse method, which penalizes sharp gradients in the viscosity parameter to prevent overfitting artifacts in the data. This comes at the expense of some smoothing of discontinuities that are physical, such as the velocity jump across the rift.

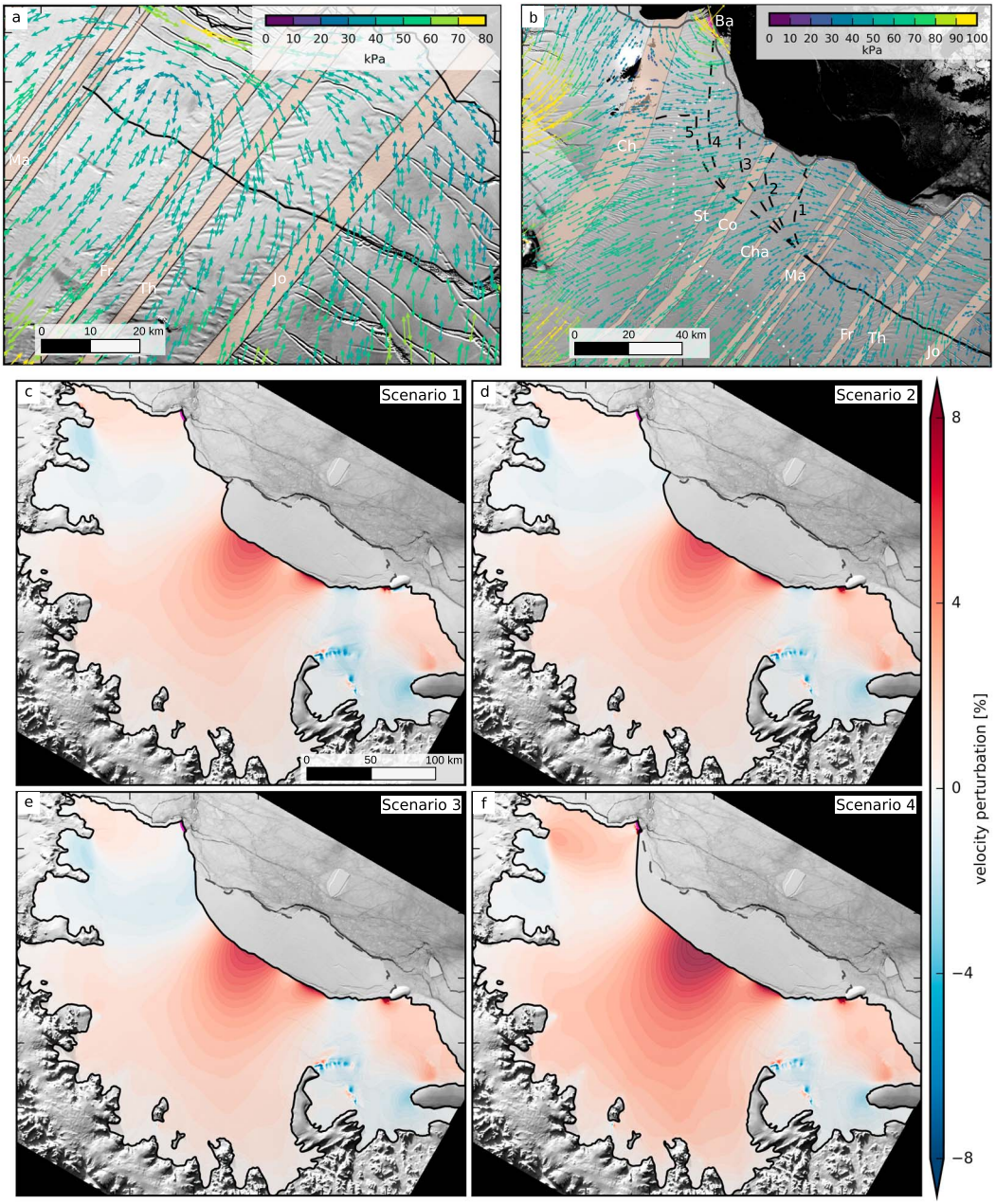

Figure 2. Modeled ice shelf stresses and postcalving velocity perturbations. (a) Magnitude and direction of maximum tensile stress from inverse modeling using earlier velocity observations [*Rignot et al.*, 2011], with eventual path of rift indicated in black. Shaded suture zones same as in Figure 1a. (b) As in Figure 2a but using 2015–2016 velocity from this study. Dashed lines indicate potential rift trajectories; dotted white line indicates compressive arch. (d–f) Velocity perturbations for different calving scenarios according to rift trajectories 1–4, identified in Figure 2b. Perturbation is expressed as a percent velocity change with respect to the initial model velocity.

The resulting model velocity field and viscosity parameter are used to calculate the stress in the ice shelf according to Glen's flow law [*Cuffey and Paterson*, 2010] with $n = 3$. To analyze the trajectory of the rift from 2014 to 2016, we also calculate stress using velocity observations [*Rignot et al.*, 2011] gathered prior to the recent propagation. Potential future rift trajectories are then outlined from stress calculations using the 2015–2016 velocity observations from this study. Both cases used the same ice thickness and surface elevation data set [*Chuter and Bamber*, 2015], boundary conditions, and initial estimate for the viscosity parameter B. Only the ice front location for the earlier velocity observations differed, as the data were masked according to an earlier, less advanced ice front. For calving perturbation scenarios, the ice shelf front is redrawn

according to the identified rift trajectories. The model velocity is then recalculated in the new shelf configuration, keeping the same spatial viscosity parameter determined in the original inverse method. We calculated only the instantaneous perturbation to the different calving scenarios; we do not consider temporal evolution subsequent to calving.

3. Results and Discussion

3.1. Rift Observations

Following a four decade period of observed stagnation, the rift of note began propagating by splitting off a preexisting rift in 2005 (Movie S1). The new rift subsequently propagated ~10 km between 2005 and 2008, before entering the Joerg Peninsula suture zone. Modest growth (<5 km) followed between 2008 and 2014, when the period of recent growth initiated [*Jansen et al.*, 2015]. Total rift growth since initiation in 2005 is ~71 km, of which ~80% has occurred since April 2014 (Figure 1 and Movie S1).

The rate of rift extension is clearly linked to the heterogeneity of the shelf, with faster rates in meteoric flow units sourced from tributary glaciers and stalled growth in the suture zones (Figure 1c). Two periods of exceptionally rapid growth (40–60 km yr^{-1}) in 2014 and 2016 occurred as the rift broke through suture zones. In both instances, rapid growth occurred during Austral winter (April–August), precluding the ability to track using visible imagery. Therefore, these propagation rates are minima and the actual rate may have been greater.

The rift leaves a clear imprint on observed flow speeds of the ice shelf (Figure 1d). The speed increases by 30% across the flanks of the rift in the south of the ice shelf, where the rift initiated and is widest. The area downstream of the rift has steadily increased in speed at a rate of 0.15 m d^{-1} yr^{-1} as the rift has opened (Figure 1e), which results from a combination of glaciological effects of ice shelf flow and kinematic effects of rotation of the nascent iceberg [*Rignot and MacAyeal*, 1989]. Melánge forming in the rift cavity may also influence ice motion downstream of the rift. Continued ice acceleration at this rate would favor continued rift growth.

3.2. Ice Shelf Stress and Velocity Simulations

For most of the 2014–2016 propagation path, the rift has traveled in a direction that is nominally orthogonal to the maximum tensile (first principal) stress direction (Figure 2a). This is consistent with observations of fracture orientation in glacier ice elsewhere [*Jansen et al.*, 2010; *Colgan et al.*, 2016]. However, the rift has a tendency to continue in the same direction as it exits a suture zone as when it entered the zone, even if this means propagating in a direction that is oblique with respect to the maximum tensile stress. For example, the rift may have been expected to turn somewhat to the left after crossing the Joerg Peninsula suture zone, given the orientation of stresses here, if not for the rapid burst of propagation upon clearing the suture zone. The propagation path also obliquely crosses a number of surface features in meteoric bands that might otherwise be expected to modify or kink the crack path. We note that the modeled stresses are viscous and are not strictly equivalent to the elastic stresses that govern fracture propagation. Therefore, we do not expect a strict adherence between rift propagation and maximum (viscous) tensile stress direction, although the viscous stresses should still be predictive of the general trend in rift trajectory.

The rapid increases in rift length after the rift crossed the Joerg Peninsula and Francis Island suture zones (Figure 1c) are consistent with a progressive increase in stresses needed to overcome the higher resistance of the suture zone. Once this resistance is overcome, the rift jumps forward into meteoric ice with lower resistance to propagation. This may explain why the rift has a tendency to continue in the same direction as it exits a suture zone as when it entered the zone, showing less sensitivity to the stress orientation and any preexisting features such as basal crevasses.

Over the most recent ~10 km of propagation (as of DOY 273, 2016), the rift appears to have begun to curve toward the ice front, consistent with encountering a stress field that would favor such a trajectory (Figure 2b). Based on the stress field from the velocity observations (Figure 2b), and the observations of rift propagation to date (nominally orthogonal to maximum tensile stress with some allowance for deviations), we outline a number of possible trajectories and resulting calving scenarios. In Scenario 1, which might be thought of as a "best-case" scenario, the rift bends sharply to align with the stress field, ultimately reaching the ice front along the Cape Chavanne suture zone. Scenario 2 represents a more gradual curving trajectory that ultimately intersects the Cole Peninsula suture zone, which has been shown to be resistant to rift propagation in the past [*McGrath et al.*, 2014]. In Scenario 3, the rift crosses the Cole Peninsula suture zone and then continues to bend

toward the ice front. Scenario 4 represents a "worst-case" scenario in which the rift propagates all the way to the Bawden Ice Rise. In order to reach the ice rise, the rift would likely have to avoid the basal crevasses that originate at Churchill Peninsula [*McGrath et al.*, 2012b] and advect all the way to Bawden.

Scenario 5 represents a case where the rift intersects one of these basal crevasses. There are two important reasons that the rift would likely arrest in such a scenario. First, the basal crevasses would be oriented nearly perpendicularly to the rift. This would favor a kinking of the rift tip. Second, the magnitude of stresses in this area is small and may not be sufficient for the rift to cross these crevasses and continue its forward trajectory. In this scenario, the rift may arrest completely, potentially intersecting the Churchill Peninsula suture zone. At this point the nascent iceberg would be quite slender and might break off somewhere to the south, leaving a "loose tooth" scenario in which the stagnant rift and a future, smaller nascent iceberg might advect for decades before encountering the higher-stress region near Bawden Ice Rise.

The velocity perturbations associated with calving events associated with Scenarios 1–4 are shown in Figures 2c–2f, respectively. In all scenarios, the model predicts that at least 70% of the ice shelf will increase in speed, with the perturbation extending all the way to the grounding line. The magnitude and spatial pattern of velocity change is similar for Scenarios 1–3. The largest perturbation is for Scenario 4, in which about 1 km of contact is lost with the Bawden Ice Rise. These scenarios represent ~40–100 km of future rift propagation. If the rift continues to propagate at the mean rate observed between April 2014 and October 2016, the ultimate calving event would be expected between July 2018 and April 2021. However, if the rift continues at the most recent, maximum rate, calving could be imminent as early as April 2017.

Previous work suggested that a future calving event associated with this rift would remove primarily "passive" shelf ice that provides limited buttressing [*Fürst et al.*, 2016]. This analysis was based on velocity perturbations to synthetic calving scenarios but did not address the question of stability. We make no attempt to define an analogous passive ice boundary, as in principle even a velocity perturbation of a few percent may cause a sufficient stress increase to destabilize additional weaknesses in the shelf.

3.3. Implications for Ice Shelf Stability

One recent study [*Jansen et al.*, 2015] suggested that this rift may pose a risk to the stability of the ice shelf, based on a notion from earlier work [*Kulessa et al.*, 2014] that the angle between the first principal (maximum tensile) stress direction and the flow direction (the "stress-flow" angle) governs the stability of fractures. In this framework, areas of low stress-flow angle are where the stress is favorably aligned to open existing weaknesses, since fractures are commonly observed to open orthogonal to the flow direction. Conversely, areas of high stress-flow angles were assumed to stabilize fractures. If the ice front retreats to an area of low stress-flow angle, it might be in a favorable position to continue retreating irreversibly.

The stress-flow angle framework considers only the direction of the maximum tensile stress, not its magnitude. Furthermore, even if the maximum tensile stress is oriented parallel to a fracture, there can still be a tensile stress component orthogonal to a fracture that would promote propagation. Indeed, classical fracture handbooks resolve the stress tensor into components parallel and perpendicular to an existing crack when calculating the stress intensity factor [e.g., *Tada et al.*, 2000].

The pattern of stress-flow angle produced by our model (Figure 3a) is more spatially complex than that presented in previous work [*Kulessa et al.*, 2014; *Jansen et al.*, 2015]. We use an inverse method to closely match modeled velocities with observed velocities, which produces a more spatially variable pattern of ice rheology than a model that uses uniform values of the viscosity parameter (B) in meteoric and marine flowbands [*Kulessa et al.*, 2014; *Jansen et al.*, 2015]. In our modeling results, it is less clear how useful the stress-flow angle concept is for defining a stable ice front position, in part due to the lack of a coherent pattern and also due to the lack of any information about stress magnitudes.

For example, the rift in question began to propagate from an area of moderate stress-flow angle (~30°, Figure 3a). In this area, the longitudinal stress that favors crack opening is about 40 kPa (Figure 3b). Many fractures upstream of the rift in question also terminate in the Joerg Peninsula suture zone. The highest longitudinal stress is across the rift furthest upstream, closest to Hollick-Kenyon Peninsula. The opening stress acting on this rift is 50% higher than across the rift that actually propagated. According to concepts of fracture mechanics these upstream fractures should be more likely to propagate than the present active rift. The fact that rifts form at the end of Hollick-Kenyon Peninsula and are subsequently stabilized for decades indicates

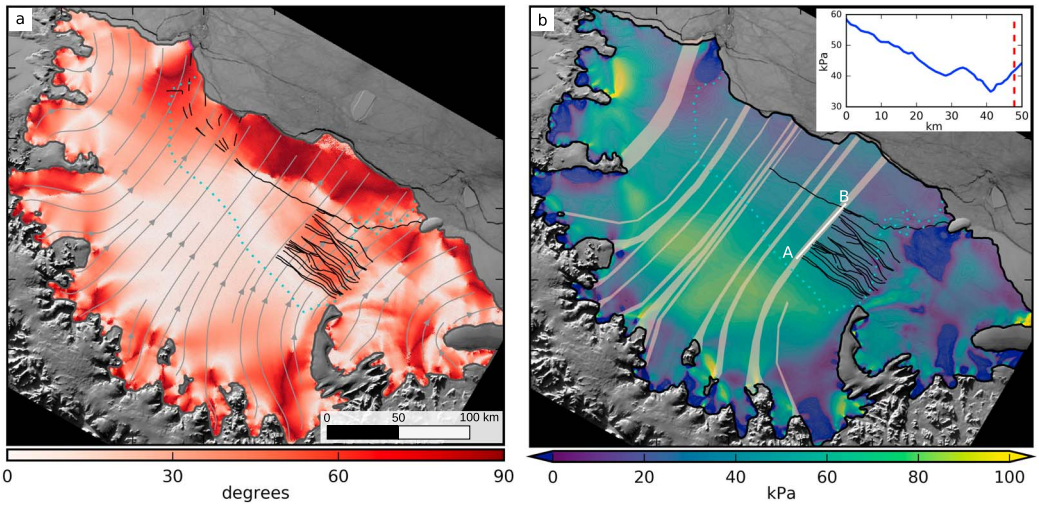

Figure 3. Stability implications for Larsen C from modeled ice shelf stresses. (a) Angle between first principal stress (Figure 2b) and the local flow direction ("stress-flow" angle). Rift extent to date and potential rift trajectories as in Figure 2b. Dotted cyan line indicates compressive arch, flow direction indicated by gray lines. Also shown are existing fractures upstream of the present rift. (b) Longitudinal (flow-parallel) stress, with suture zones indicated as in Figure 2. Inset shows stress along profile A-B; red dashed line indicates location of present rift.

that the Joerg Peninsula suture zone must have higher resistance to fracture than the meteoric ice from which the rifts originated. This underscores the critical role that this suture zone plays in stabilizing the ice shelf.

3.4. Fracture Toughness of Suture Zones

Observations of rift propagation across suture zones (Figure 1) and arrest within suture zones (Figure 3) indicate that these areas have higher fracture toughness, a term relating to a material's resistance to fracture. In any material, increasing heterogeneity causes crack tip blunting, leading to higher load bearing capacity [*Bažant and Planas*, 1998; *Borstad and McClung*, 2011]. Higher fracture toughness of suture zones is thus consistent with observations of the heterogeneous composition of these zones [*McGrath et al.*, 2014] and widespread observations of fractures arresting along these boundaries [*Glasser et al.*, 2009; *Hulbe et al.*, 2010; *McGrath et al.*, 2012a; *Jansen et al.*, 2013], which by definition indicates that the stress intensity factor no longer exceeds the fracture toughness. Quantifying the bulk fracture toughness of suture zones relative to meteoric ice, for which fracture toughness is known [*Rist et al.*, 2002], would improve model predictions of ice shelf fracturing and stability.

Suture zones evolve longitudinally in an ice shelf. In the positive surface mass balance regime that typifies many Antarctic ice shelves, the fraction of a suture zone composed of heterogeneous ice (accreted marine ice, sea ice, fallen meteoric blocks, and in situ snowfall) decreases as a percentage of the ice shelf thickness toward the ice front [*Kulessa et al.*, 2014; *McGrath et al.*, 2014]. Increases in basal melting would reduce the amount of heterogeneous ice in a suture zone, reducing the column average fracture toughness and making it easier for a rift to propagate. Scant observations preclude a determination of whether this is a plausible explanation for the recent growth of this rift in Larsen C.

4. Conclusions

A quickly evolving rift represents a potential threat to the stability of the Antarctic Peninsula's largest ice shelf. The rift propagation rate is clearly linked to the alternating bands of meteoric ice and suture zones encountered by the fracture. We present evidence that suture zones have higher fracture toughness, a finding that prompts a necessary revision of existing theories of ice shelf stability.

We assimilate new velocity observations in an ice sheet model to determine the stresses in the ice shelf and outline plausible rift trajectories. The rift is likely to bend toward the ice front given the orientation of the stresses ahead of the current rift tip. All plausible calving scenarios would lead to widespread, even if moderate, acceleration, with perturbations likely reaching the grounding line. This represents the closest to real-time analysis of the state of stress of any ice shelf, and in finer spatial detail, yet presented.

Without the stabilizing influence of the Joerg Peninsula suture zone, the Larsen C ice shelf would probably not exist in its present form, if at all. As soon as a rift formed at the end of Hollick-Kenyon Peninsula, it would likely propagate across the ice shelf, well within the compressive arch. The future stability of Larsen C thus depends on the factors that allowed the present rift to punch through this suture zone, which had previously stabilized dozens of fractures for decades. This is likely a more important consideration for the stability of Larsen C than any definition of a stable ice front position. Since ice shelves retreat and collapse following the formation and propagation of fractures, we conclude that any theory of ice shelf stability must account for the role that ice heterogeneity plays in controlling fracture propagation.

Acknowledgments
We thank Ted Scambos, Rick Aster, Paul Holland, Martin O'Leary, Karen Alley, and two anonymous reviewers for their valuable comments. Paul Holland provided the Larsen C suture zone definitions. Thanks to the data providers, including the National Snow and Ice Data Center which provides freely available image velocity maps derived from Landsat 8 using PyCorr for Larsen C and all other glacier ice on the planet (https://nsidc.org/data/golive). Any use of trade, firm, or product names is for descriptive purposes only and does not imply endorsement by the U.S. Government. A. Pope was supported by USGS contract G12PC00066. Workflow and code for the velocity processing is publicly available [*Pope*, 2016]. The source code for the model used in this study, the Ice Sheet System Model (ISSM), is freely available at issm.jpl.nasa.gov. Version 4.11 of ISSM, svn revision 21205, was used in this study. The input files and data necessary to reproduce the results using ISSM are available from the authors upon request (chris.borstad@unis.no).

References

Banwell, A. F., D. R. MacAyeal, and O. V. Sergienko (2013), Breakup of the Larsen B Ice Shelf triggered by chain reaction drainage of supraglacial lakes, *Geophys. Res. Lett.*, *40*, 5872–5876, doi:10.1002/2013GL057694.

Bassis, J. N., H. A. Fricker, R. Coleman, and J.-B. Minster (2008), An investigation into the forces that drive ice-shelf rift propagation on the Amery Ice Shelf, East Antarctica, *J. Glaciol.*, *54*(184), 17–27.

Bažant, Z. P., and J. Planas (1998), *Fracture and Size Effect in Concrete and Other Quasibrittle Materials*, 640 pp., CRC Press, Boca Raton, Fla.

Berthier, E., T. A. Scambos, and C. A. Shuman (2012), Mass loss of Larsen B tributary glaciers (Antarctic Peninsula) unabated since 2002, *Geophys. Res. Lett.*, *39*, L13501, doi:10.1029/2012GL051755.

Borstad, C. P., and D. M. McClung (2011), Numerical modeling of tensile fracture initiation and propagation in snow slabs using nonlocal damage mechanics, *Cold Reg. Sci. Technol.*, *69*, 145–155, doi:10.1016/j.coldregions.2011.09.010.

Borstad, C. P., A. Khazendar, E. Larour, M. Morlighem, E. Rignot, M. P. Schodlok, and H. Seroussi (2012), A damage mechanics assessment of the Larsen B ice shelf prior to collapse: Toward a physically-based calving law, *Geophys. Res. Lett.*, *39*, L18502, doi:10.1029/2012GL053317.

Borstad, C. P., E. Rignot, J. Mouginot, and M. P. Schodlok (2013), Creep deformation and buttressing capacity of damaged ice shelves: Theory and application to Larsen C ice shelf, *Cryosphere*, *7*(4), 1931–1947, doi:10.5194/tc-7-1931-2013.

Chuter, S. J., and J. L. Bamber (2015), Antarctic ice shelf thickness from CryoSat-2 radar altimetry, *Geophys. Res. Lett.*, *42*, 10,721–10,729, doi:10.1002/2015GL066515.

Colgan, W., H. Rajaram, W. Abdalati, C. Mccutchan, R. Mottram, M. Moussavi, and S. Grigsby (2016), Glacier crevasses: Observations, models and mass balance implications, *Rev. Geophys.*, *54*, 119–161, doi:10.1002/2015RG000504.

Cuffey, K. M., and W. S. B. Paterson (2010), *The Physics of Glaciers* 4th edn., Elsevier, Oxford, U. K.

Depoorter, M. A., J. L. Bamber, J. A. Griggs, J. T. M. Lenaerts, S. R. M. Ligtenberg, M. R. van den Broeke, and G. Moholdt (2013), Calving fluxes and basal melt rates of Antarctic ice shelves, *Nature*, *502*(7469), 89–92, doi:10.1038/nature12567.

Doake, C. S. M., and D. G. Vaughan (1991), Rapid disintegration of the Wordie Ice Shelf in response to atmospheric warming, *Nature*, *350*(6316), 328–330.

Doake, C. S. M., H. F. J. Corr, H. Rott, P. Skvarca, and N. W. Young (1998), Breakup and conditions for stability of the northern Larsen Ice Shelf, Antarctica, *Nature*, *391*(6669), 778–780, doi:10.1038/35832.

Fahnestock, M., T. Scambos, T. Moon, A. Gardner, T. Haran, and M. Klinger (2016), Rapid large-area mapping of ice flow using Landsat 8, *Remote Sens. Environ.*, *185*, 84–94, doi:10.1016/j.rse.2015.11.023.

Fretwell, P., et al. (2013), Bedmap2: Improved ice bed, surface and thickness datasets for Antarctica, *Cryosphere*, *7*(1), 375–393, doi:10.5194/tc-7-375-2013.

Fricker, H. A., N. W. Young, R. Coleman, J. N. Bassis, and J. B. Minster (2005), Multi-year monitoring of rift propagation on the Amery Ice Shelf, East Antarctica, *Geophys. Res. Lett.*, *32*, L02502, doi:10.1029/2004GL021036.

Fürst, J. J., G. Durand, F. Gillet-Chaulet, L. Tavard, M. Rankl, M. Braun, and O. Gagliardini (2016), The safety band of Antarctic ice shelves, *Nat. Clim. Change*, *6*, 479–482, doi:10.1038/NCLIMATE2912.

Glasser, N. F., and T. A. Scambos (2008), A structural glaciological analysis of the 2002 Larsen B ice-shelf collapse, *J. Glaciol.*, *54*(184), 3–16.

Glasser, N. F., B. Kulessa, A. Luckman, D. Jansen, E. C. King, P. R. Sammonds, T. A. Scambos, and K. C. Jezek (2009), Surface structure and stability of the Larsen C ice shelf, Antarctic Peninsula, *J. Glaciol.*, *55*(191), 400–410.

Holland, P. R., H. F. J. Corr, D. G. Vaughan, A. Jenkins, and P. Skvarca (2009), Marine ice in Larsen Ice Shelf, *Geophys. Res. Lett.*, *36*, L11604, doi:10.1029/2009GL038162.

Holland, P. R., A. Brisbourne, H. F. J. Corr, D. McGrath, K. Purdon, J. Paden, H. A. Fricker, F. S. Paolo, and A. H. Fleming (2015), Oceanic and atmospheric forcing of Larsen C Ice-Shelf thinning, *Cryosphere*, *9*(3), 1005–1024, doi:10.5194/tc-9-1005-2015.

Hulbe, C. L., C. LeDoux, and K. Cruikshank (2010), Propagation of long fractures in the Ronne Ice Shelf, Antarctica, investigated using a numerical model of fracture propagation, *J. Glaciol.*, *56*(197), 459–472.

Jansen, D., B. Kulessa, P. R. Sammonds, A. Luckman, E. C. King, and N. F. Glasser (2010), Present stability of the Larsen C ice shelf, Antarctic Peninsula, *J. Glaciol.*, *56*(198), 593–600.

Jansen, D., A. Luckman, B. Kulessa, P. R. Holland, and E. C. King (2013), Marine ice formation in a suture zone on the Larsen C Ice Shelf and its influence on ice shelf dynamics, *J. Geophys. Res. Earth Surf.*, *118*, 1628–1640, doi:10.1002/jgrf.20120.

Jansen, D., A. J. Luckman, A. Cook, S. Bevan, B. Kulessa, B. Hubbard, and P. R. Holland (2015), Brief communication: Newly developing rift in Larsen C Ice Shelf presents significant risk to stability, *Cryosphere*, *9*(3), 1223–1227, doi:10.5194/tc-9-1223-2015.

Joughin, I., and D. R. MacAyeal (2005), Calving of large tabular icebergs from ice shelf rift systems, *Geophys. Res. Lett.*, *32*, L02501, doi:10.1029/2004GL020978.

Kulessa, B., D. Jansen, A. J. Luckman, E. C. King, and P. R. Sammonds (2014), Marine ice regulates the future stability of a large Antarctic ice shelf, *Nat. Commun.*, *5*, 3707, doi:10.1038/ncomms4707.

Larour, E., E. Rignot, I. Joughin, and D. Aubry (2005), Rheology of the Ronne Ice Shelf, Antarctica, inferred from satellite radar interferometry data using an inverse control method, *Geophys. Res. Lett.*, *32*, L05503, doi:10.1029/2004GL021693.

Larour, E., H. Seroussi, M. Morlighem, and E. Rignot (2012), Continental scale, high order, high spatial resolution, ice sheet modeling using the Ice Sheet System Model (ISSM), *J. Geophys. Res.*, *117*, F01022, doi:10.1029/2011JF002140.

Luckman, A., D. Jansen, B. Kulessa, E. C. King, P. Sammonds, and D. I. Benn (2012), Basal crevasses in Larsen C Ice Shelf and implications for their global abundance, *Cryosphere*, *6*(1), 113–123, doi:10.5194/tc-6-113-2012.

Matsuoka, K., et al. (2015), Antarctic ice rises and rumples: Their properties and significance for ice-sheet dynamics and evolution, *Earth Sci. Rev.*, *150*, 724–745, doi:10.1016/j.earscirev.2015.09.004.

McGrath, D., K. Steffen, H. Rajaram, T. Scambos, W. Abdalati, and E. Rignot (2012a), Basal crevasses on the Larsen C Ice Shelf, Antarctica: Implications for meltwater ponding and hydrofracture, *Geophys. Res. Lett.*, *39*, L16504, doi:10.1029/2012GL052413.

McGrath, D., K. Steffen, T. Scambos, H. Rajaram, G. Casassa, and J. L. Rodriguez Lagos (2012b), Basal crevasses and associated surface crevassing on the Larsen C ice shelf, Antarctica, and their role in ice-shelf instability, *Ann. Glaciol.*, *53*(60), 10–18, doi:10.3189/2012AoG60A005.

McGrath, D., K. Steffen, P. R. Holland, T. Scambos, H. Rajaram, W. Abdalati, and E. Rignot (2014), The structure and effect of suture zones in the Larsen C Ice Shelf, Antarctica, *J. Geophys. Res. Earth Surf.*, *119*, 588–602, doi:10.1002/2013JF002935.

Mercer, J. H. (1978), West Antarctic ice sheet and CO_2 greenhouse effect: A threat of disaster, *Nature*, *271*, 321–325, doi:10.1038/271321a0.

Morlighem, M., H. Seroussi, E. Larour, and E. Rignot (2013), Inversion of basal friction in Antarctica using exact and incomplete adjoints of a higher-order model, *J. Geophys. Res. Earth Surf.*, *118*, 1746–1753, doi:10.1002/jgrf.20125.

Pope, A. (2016), allenpope/Landsat8_Velocity_LarsenC: Processing Landsat 8 velocities for Larsen C [Data set]. Zenodo, [Available at http://doi.org/10.5281/zenodo.185651.]

Rignot, E., and D. R. MacAyeal (1989), Ice-shelf dynamics near the front of the Filchner-Ronne Ice Shelf, Antarctica, revealed by SAR interferometry, *J. Glaciol.*, *44*(147), 405–418.

Rignot, E., G. Casassa, P. Gogineni, W. Krabill, A. Rivera, and R. Thomas (2004), Accelerated ice discharge from the Antarctic Peninsula following the collapse of Larsen B ice shelf, *Geophys. Res. Lett.*, *31*, L18401, doi:10.1029/2004GL020697.

Rignot, E., J. Mouginot, and B. Scheuchl (2011), Ice flow of the Antarctic Ice Sheet, *Science*, *333*(6048), 1427–1430, doi:10.1126/science.1208336.

Rist, M. A., P. R. Sammonds, H. Oerter, and C. S. M. Doake (2002), Fracture of Antarctic shelf ice, *J. Geophys. Res.*, *107*(B1), 2002, doi:10.1029/2000JB000058.

Scambos, T. A., J. A. Bohlander, C. A. Shuman, and P. Skvarca (2004), Glacier acceleration and thinning after ice shelf collapse in the Larsen B embayment, Antarctica, *Geophys. Res. Lett.*, *31*, L18402, doi:10.1029/2004GL020670.

Scambos, T. A., E. Berthier, T. Haran, C. A. Shuman, A. J. Cook, S. R. M. Ligtenberg, and J. Bohlander (2014), Detailed ice loss pattern in the northern Antarctic Peninsula: Widespread decline driven by ice front retreats, *Cryosphere*, *8*(6), 2135–2145, doi:10.5194/tc-8-2135-2014.

Tada, H., P. C. Paris, and G. R Irwin (2000), *The Stress Analysis of Cracks Handbook*,ASME Press, New York, doi:10.1115/1.801535.

Vieli, A., A. J. Payne, A. Shepherd, and Z. Du (2007), Causes of pre-collapse changes of the Larsen B ice shelf: Numerical modelling and assimilation of satellite observations, *Earth Planet. Sci. Lett.*, *259*(3–4), 297–306, doi:10.1016/j.epsl.2007.04.050.

Walker, C. C., J. N. Bassis, H. A. Fricker, and R. J. Czerwinski (2015), Observations of interannual and spatial variability in rift propagation in the Amery Ice Shelf, Antarctica, 2002–14, *J. Glaciol.*, *61*(226), 243–252, doi:10.3189/2015JoG14J151.

Wuite, J., H. Rott, M. Hetzenecker, D. Floricioiu, J. De Rydt, G. H. Gudmundsson, T. Nagler, and M. Kern (2015), Evolution of surface velocities and ice discharge of Larsen B outlet glaciers from 1995 to 2013, *Cryosphere*, *9*(3), 957–969, doi:10.5194/tc-9-957-2015.